ChemBioChem

Research Article
doi.org/10.1002/cbic.202400756

Chemistry Europe
European Chemical Societies Publishing

www.chembiochem.org

Mitochondrial Viscosity Probes: Iridium(III) Complexes Induce Apoptosis in HeLa Cells

Bingbing Chen[†,[a, c]] Zhijun Liang[†,[a]] Yao Gong[†,[a]] Wei Wu,[[a]] Jiaen Huang,[[a]] Jiaxi Chen,*[[a]] Yanmei Wang,[[a]] Jun Mei,[[a]] Rui Chen,*[[a]] Zunnan Huang,[[b]] and Jing Sun*[[a, b]]

Mitochondrial viscosity has emerged as a promising biomarker for diseases such as cancer and neurodegenerative disorders, yet accurately measuring viscosity at the subcellular level remains a significant challenge. In this study, we synthesized and characterized three cyclometalated iridium(III) complexes (**Ir1-Ir3**) containing 5-fluorouracil derivatives as ligands. Among these, **Ir1** selectively induced apoptosis in HeLa cells by increasing mitochondrial production of reactive oxygen species (ROS), which triggered a cascade of events leading to mitochondrial dysfunction. Additionally, the fluorescence lifetime of **Ir1** demonstrated high sensitivity to intracellular viscosity changes, enabling real-time fluorescence lifetime imaging microscopy (FLIM) of cellular micro-viscosity during apoptosis. These findings underscore the potential of cyclometalated Ir(III) complexes for both therapeutic and diagnostic applications at the subcellular level.

1. Introduction

Cancer represents a growing global health and economic challenge, with incidence rates projected to increase significantly in the coming years. Although cisplatin remains a cornerstone of anticancer therapy, its efficacy is often compromised by drug resistance and severe side effects,[1–3] prompting the search for alternative therapies involving other transition metals. Among these, iridium has attracted considerable attention due to its distinctive properties, including its ability to form stable complexes suitable for targeted therapies. Iridium complexes offer several advantages, such as tunable configurations, exceptional photophysical properties, organelle-targeting capabilities and distinct antitumor mechanisms.[4,5] For example, Ir(III) complexes can be designed to target specific organelles through molecular design and structural modifications.[6,7] Furthermore, these complexes can detect various environmental changes, such as shifts in pH,[8,9] oxygen levels[10,11] and viscosity.[12,13] However, their application as fluorescence probes has been limited by low sensitivity to external factors, including concentration and solvent conditions.[14]

Fluorescence lifetime, an intrinsic characteristic of fluorescent molecules, is highly sensitive to changes in the molecular microenvironment. Fluorescence lifetime imaging microscopy (FLIM), a non-invasive and minimally destructive technique, enables precise monitoring and visualization of these changes within cells,[15] offering high specificity and sensitivity while remaining unaffected by common issues such as photobleaching, excitation variability and fluorescence intensity fluctuations.[16] Additionally, FLIM probes with viscosity-dependent lifetimes can provide quantitative insights into cellular states, such as inflammation and programmed cell death.

Mitochondria, often referred to as the "powerhouses" of the cell, play a critical role in maintaining cellular metabolism and homeostasis.[17] Changes in mitochondrial viscosity are closely linked to physiological processes, including metabolite diffusion, electron transport, apoptosis, autophagy, mitosis and protein-protein interactions.[18,19] Importantly, mitochondrial viscosity has been identified as a potential biomarker for several diseases, including cancer,[20] Huntington's disease[21] and Alzheimer's disease.[22,23]

In this study, we aimed to leverage the unique photophysical properties of cyclometallic Ir(III) complexes incorporating 1-(4-((1,10-phenanthrolin-5-yl)amino)butyl)-5-fluoropyrimidine-2,4(1H,3H)-dione (L) as a ligand to detect mitochondrial viscosity while inducing antitumor activity. Three Ir(III) complexes were synthesized, each incorporating a different compound represented as (C–N) in the chemical formula $[Ir(C–N)_2L]PF_6$: **Ir1** (1-phenylisoquinoline, piq), **Ir2** (7,8-benzoquinoline, bzq) and **Ir3** (2-(2-thienyl)pyridine, thpy). **Ir1** specifically targeted mitochondria in HeLa cells, inducing apoptosis by generating reactive oxygen species (ROS), which triggered a cascade of events leading to mitochondrial dysfunction. Additionally, the fluorescent properties of **Ir1** enabled quantitative, real-time monitoring of changes in mitochondrial viscosity through FLIM. This study highlights the

[a] B. Chen, Z. Liang, Y. Gong, W. Wu, J. Huang, J. Chen, Y. Wang, J. Mei, R. Chen, J. Sun
The First Dongguan Affiliated Hospital, School of Pharmacy, Guangdong Medical University, Dongguan 523808, China
Tel.: +86-769-2289-6322
E-mail: jiaxi@gdmu.edu.cn
415317456@qq.com
sunjing03@foxmail.com

[b] Z. Huang, J. Sun
Key Laboratory of Computer-Aided Drug Design of Dongguan City, Guangdong Medical University, Dongguan 523808, China

[c] B. Chen
Key Laboratory of Luminescence Analysis and Molecular Sensing, College of Pharmaceutical Sciences, Southwest University, Chongqing 400715, China

[†] Contributed equally to this work.

Supporting information for this article is available on the WWW under https://doi.org/10.1002/cbic.202400756

potential of cyclometallic Ir(III) complexes to induce and precisely monitor microenvironmental changes at the subcellular level, offering valuable insights for therapeutic and diagnostic applications (Figure 1).

2. Results and Discussion

2.1. Synthesis and Characterization

Ligand L was synthesized following our previously established method.[24] The synthesis of complexes **Ir1**-**Ir3** is outlined in Scheme 1. Briefly, two equivalents of ligand L were refluxed with a chlorine-bridged Ir(III) dimer. The resulting complexes **Ir1**-**Ir3**, were characterized via elemental analysis, ESI-MS, and ^{1}H NMR, as shown in Figure S1–S6. The UV-Vis absorption spectra of **Ir1**-**Ir3** in phosphate-buffered saline (PBS), CH_2Cl_2 and CH_3CN exhibited pronounced absorption in the 270–300 nm range, corresponding to spin-allowed intra-ligand electron transitions, and weaker absorption in the 400–450 nm range, indicative of a metal-to-ligand electronic transition (Figure S7). Upon excitation at 405 nm, all complexes emitted light in PBS, CH_2Cl_2 and CH_3CN at 298 K (Figure S8).

2.2. Viscosity-Sensitive Emission Properties

To evaluate the viscosity-sensitive properties of complexes **Ir1**-**Ir3**, we examined their fluorescence intensity and lifetime in various solvent mixtures of methanol and glycerol. As shown in Figure 2, all three complexes displayed viscosity-dependent changes in both fluorescence intensity and fluorescence lifetime (*T*). Notably, the fluorescence intensity of **Ir1** in 80% glycerol was 10.2 times higher than in methanol, while **Ir2** and **Ir3** showed 8.73-fold and 4.09-fold increases, respectively. As the glycerol concentration increased to 90%, the *T* values for **Ir1**, **Ir2** and **Ir3** increased from 0.35 μs to 3.2 μs, 0.15 μs to 1.26 μs and 0.12 μs to 4.5 μs, respectively. A direct linear correlation was observed between the T values of **Ir1**-**Ir3** and the solvent viscosity parameter (η), consistent with the range of viscosities reported in cellular environments.[25,26] Overall, all three complexes exhibited enhanced photophysical properties, with **Ir1** demonstrating the most significant increase in fluorescence intensity, prompting further studies on its physical properties.

To confirm the specificity of **Ir1**'s response to viscosity, we evaluated its fluorescence lifetime under various conditions. Increasing the proportion of 1,4-dioxane in water from 25% to 100% resulted in minimal changes in the T value of **Ir1** (Figure S9). Additionally, its fluorescence lifetime showed only slight responses to variations in solvent type, glutathione (GSH) content and human serum albumin (HSA) content (Figure S10).

2.3. Cytotoxicity Assay

The cytotoxicities of the **Ir1**-**Ir3** were assessed against various tumor cell lines, including HeLa (human cervical carcinoma), HepG2 (human hepatocellular carcinoma), MCF-7 (Michigan Cancer Foundation-7, human breast carcinoma), Caco-2 (human colon adenocarcinoma) and KYSE-140 (human esophageal squamous cell carcinoma). All three modified 5-Fu–Ir(III) complexes exhibited significantly enhanced antitumor activity in HeLa cells compared to 5-Fu alone (Table 1). Among them, **Ir1** exhibited the strongest antiproliferative effect, with an IC_{50} value of 3 μM against HeLa cells. Given **Ir1**'s excellent photophysical properties and potent antitumor activity, it was selected for further mechanistic studies.

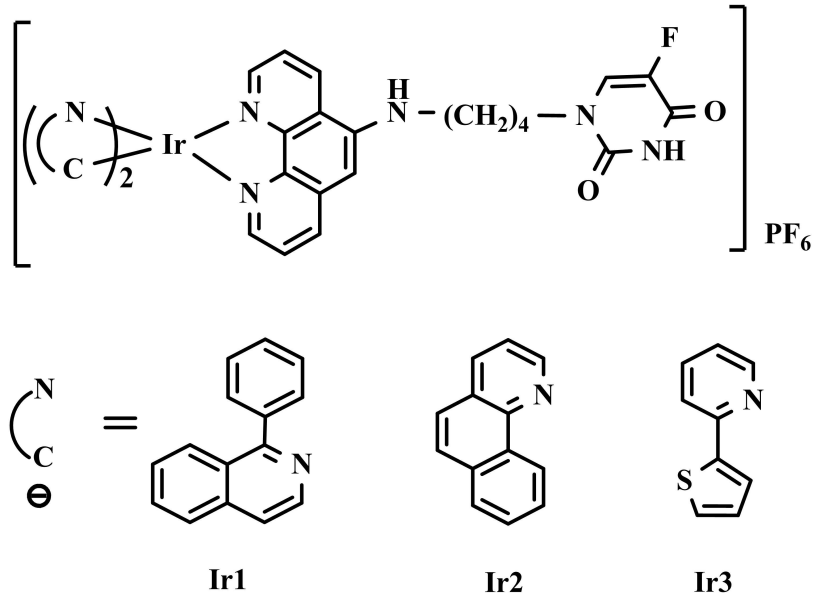

Figure 1. The structures of complexes **Ir1**-**Ir3**.

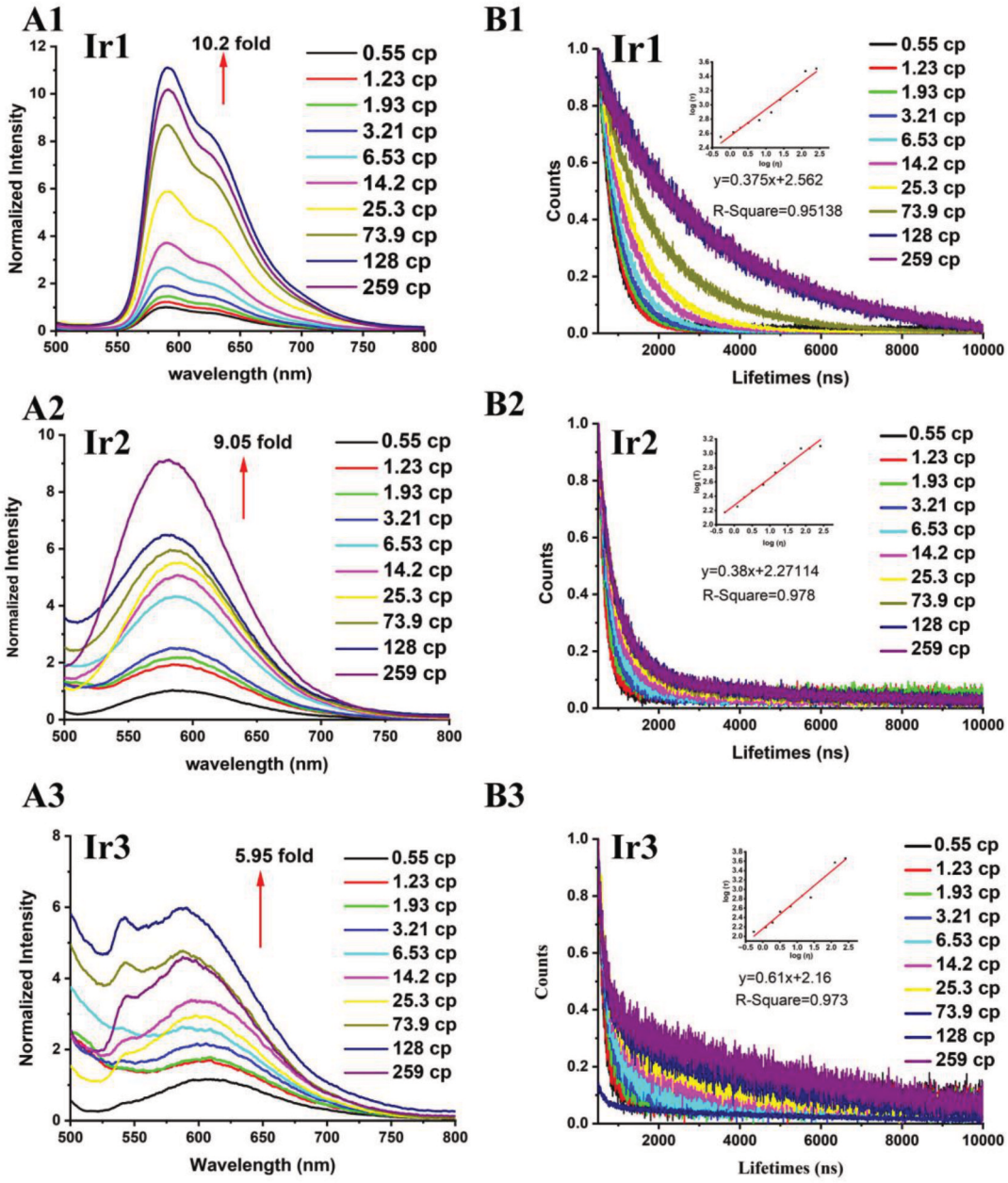

Figure 2. Emission intensity (A) and lifetime (B) of complexes **Ir1**-**Ir3** measured in mixtures of CH_3OH and glycerol (percentage of glycerol = 0%, 10%, 20%, 30%, 40%, 50%, 60%, 70%, 80 and 90%, *v*/*v*, λ_{ex} = 405 nm). The arrow shows the intensity variations with an increasing proportion of glycerol.

Table 1. IC_{50} values of tested compounds towards different cell lines.[a]

Compounds	IC_{50} (μM)				
	HeLa	$HepG_2$	MCF-7	Caco-2	KYSE-140
Ir1	3.0 ± 0.1	105.6 ± 4.6	9.3 ± 1.3	14.6 ± 1.7	6.1 ± 0.2
Ir2	5.4 ± 0.1	129.1 ± 5.8	34.2 ± 3.1	21.8 ± 2.0	14.9 ± 1.9
Ir3	6.4 ± 0.3	77.3 ± 3.8	53.8 ± 4.2	19.6 ± 5.5	19.3 ± 2.5
5-Fu	47.9 ± 1.7	42.1 ± 2.3	65.0 ± 2.6	11.4 ± 1.0	58.6 ± 3.3

[a] IC_{50} values are drug concentrations necessary for 50% inhibition of cell viability. Data are presented as ± standard deviations obtained in at least three independent experiments and treatment period was 48 h.

2.4. Intracellular Localization

Based on their excellent photophysical properties, we utilized fluorescence microscopy to visualize the subcellular distributions of Ir(III) complexes. Confocal microscopy images (Figure S11) revealed that **Ir1** accumulated in the cytoplasm after 5 hours of treatment. Given that mechanistic studies suggest small molecules like **Ir1** enter cells via energy-dependent pathways, we conducted confocal microscopy on HeLa cells exposed to **Ir1** at a low temperature (4 °C) and observed reduced uptake efficiency (Figure S12), confirming an energy-dependent uptake mechanism.

Previous studies have reported that Ir(III) complexes localize to specific organelles, such as mitochondria or lysosomes.[27,28] To further investigate **Ir1** localization in HeLa cells, we used MitoTracker Red (MTR) and LysoTracker Red (LTR) dyes. After a 5-hour incubation, **Ir1** showed substantial colocalization with MTR, as indicated by a Pearson's correlation coefficient (PCC) of 0.94, which was significantly higher than its colocalization with LTR (PCC = 0.39) (Figure 3), demonstrating the selective mitochondrial localization of **Ir1**.

2.5. Apoptosis Induction

Given **Ir1**'s superior antitumor activity compared to 5-Fu, we further investigated its mechanism of action. Apoptosis is characterized by distinct morphological changes, including cell shrinkage, mitochondrial swelling, formation of apoptotic bodies and nuclear fragmentation.[27] Confocal microscopy data (Figure 4A) showed that treatment of HeLa cells with **Ir1** led to dose-dependent nuclear damage, with significant nuclear fragmentation occurring at higher **Ir1** concentrations. Consistent with these findings, Annexin V-FITC staining revealed a concentration-dependent increase in the proportion of apoptotic cells following 24-hour **Ir1** treatment, rising from 0.76 ± 0.08 % at 0 μM to 59.75 ± 2.33 % at 6 μM **Ir1** (Figure 4B).

Caspase proteins play a crucial role in the regulation of apoptosis and can be categorized into initiator caspases (e.g., caspase 8 and caspase 9) and executioner caspases (e.g., caspase 3 and caspase 7) based on their functions.[28] During apoptotic stress, increased mitochondrial outer membrane permeability allows the release of apoptotic proteins from the intermembrane space into the cytoplasm. This release subsequently activates caspases 3 and 7, initiating apoptosis. Therefore, elevated levels of caspase 3/7 activity are indicative of apoptosis induction.[29,30] Following 24-hour treatment of HeLa cells with **Ir1**, we observed a dose-dependent increase in caspase 3/7 activity, with the highest concentration group showing a 2.82-fold increase compared to the control group (Figure 4C). These findings collectively suggest that **Ir1** induces apoptosis in HeLa cells through a caspase-dependent mitochondrial pathway.

2.6. Intracellular ROS Level

Research has demonstrated that elevated ROS levels can damage tumor cells and induce apoptosis.[31,32] To assess this effect, HeLa cells were incubated with **Ir1** at concentrations of 2, 4 and 6 μM for 12 hours, and intracellular ROS levels were measured using H_2DCF-DA staining. Flow cytometry results (Figure 5A) showed that ROS levels in the highest concentration group were 5.7 times greater than those in the control group. Confocal microscopy confirmed a concentration-dependent increase in intracellular ROS levels (Figure 5B), consistent with the flow cytometry findings. The fluorescence intensity of the DCF probe within the cells also exhibited a concentration-dependent increase, suggesting that **Ir1** can induce a significant rise in ROS production in HeLa cells.

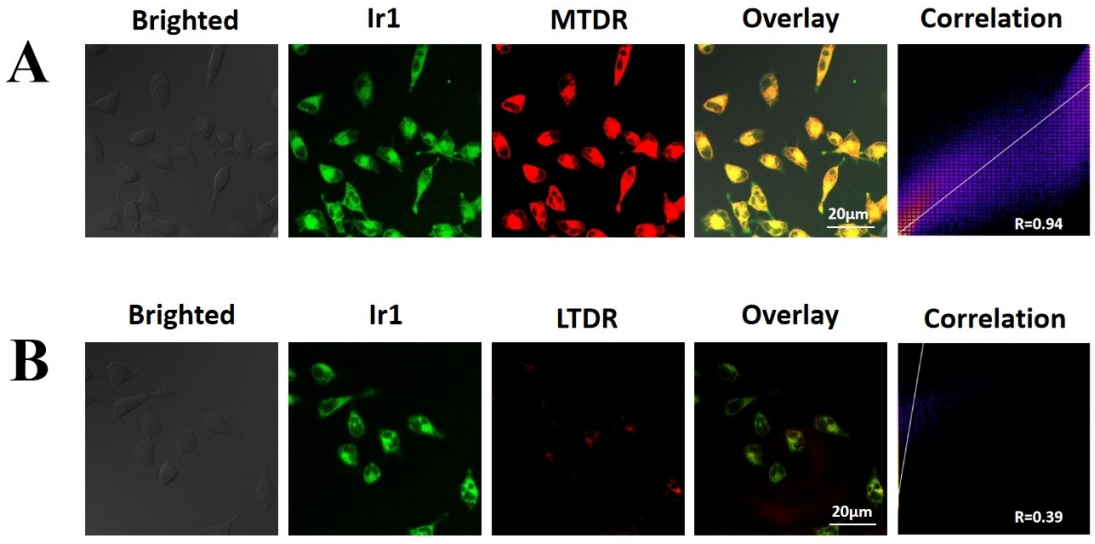

Figure 3. Confocal microscopy images of HeLa cells co-labeled with **Ir1** (2 μM, 5 h), MTR (100 nM, 0.5 h) and LTR (100 nM, 0.5 h). The excitation of **Ir1** was 405 nm, whereas MTR and LTR were 552 nm.

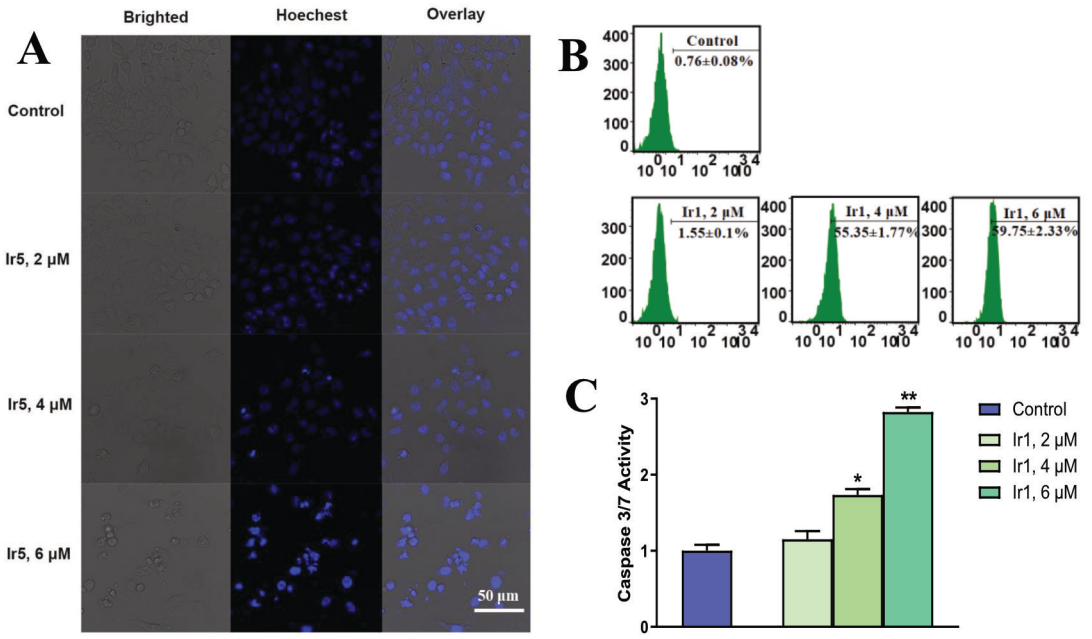

Figure 4. (A) Confocal microscopic images of HeLa cells incubated with **Ir1** (2, 4, 6 μM, 24 h) and stained with Hoechst 33342 (5 μg/mL, 30 min). λ_{ex} = 405 nm; λ_{em} = 406 ± 20 nm. (B) Flow-cytometric quantification of Annexin V-FITC (FITC: fluoresceine isothiocyanate) labeled HeLa cells treated with **Ir1** at different concentrations for 24 h. (C) Activation of caspase 3/7. HeLa cells were exposed to **Ir1** at different concentrations for 24 h. (*$p < 0.05$, **$p < 0.01$, n = 9)

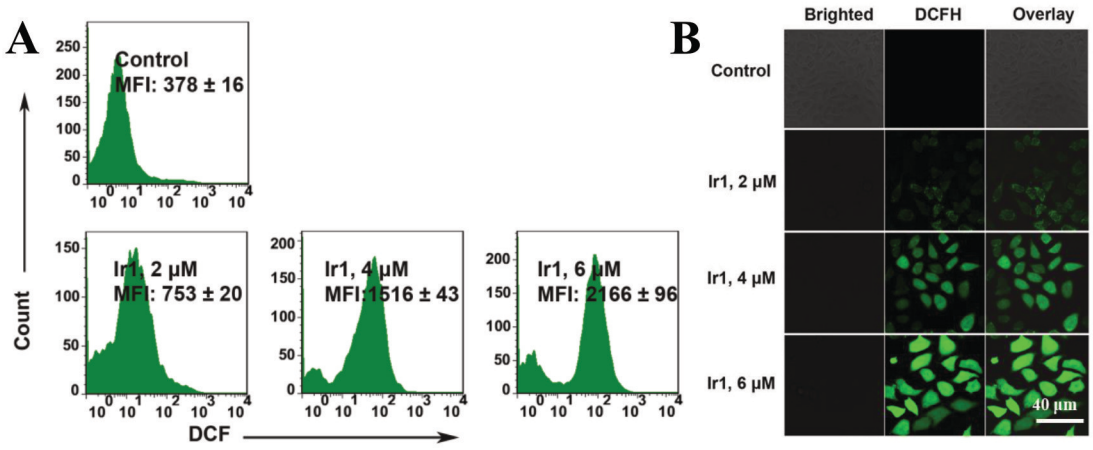

Figure 5. Effects of **Ir1** on ROS generation. HeLa cells were treated with **Ir1** at different concentrations for 24 h, and stained by DCFH-DA. Samples were detected by flow cytometryy (A) and confocal microscop (B).

2.7. Cell-Cycle Arrest

Iridium-based transition metal complexes and the conventional anti-cancer drug 5-Fu typically induce apoptosis by damaging DNA,[33,34] prompting us to use flow cytometry to assess DNA content in **Ir1**-treated HeLa cells. After HeLa cells were treated with 2, 4 and 6 μM **Ir1** for 24 hours, a significant proportion of cells were arrested in the S phase of the cell cycle (Control: 46.04 ± 1.04%; 6 μM **Ir1**: 55.46 ± 1.41%), accompanied by a marked reduction in the percentage of cells in the G1/G0 phase (Control: 34.05 ± 0.39%; 6 μM **Ir1**: 17.28 ± 1.45%) (Figure 6 and Table S1). These findings indicate that **Ir1** induces apoptosis by targeting actively replicating DNA and arresting cells in the S phase, reinforcing DNA damage as a key mechanism underlying its antitumor activity.

2.8. Mitochondrial Dysfunction

Mitochondria are essential for ATP production via the tricarboxylic acid cycle;[35,36] therefore, disruption of mitochondrial function reduces ATP production, impairing cellular processes

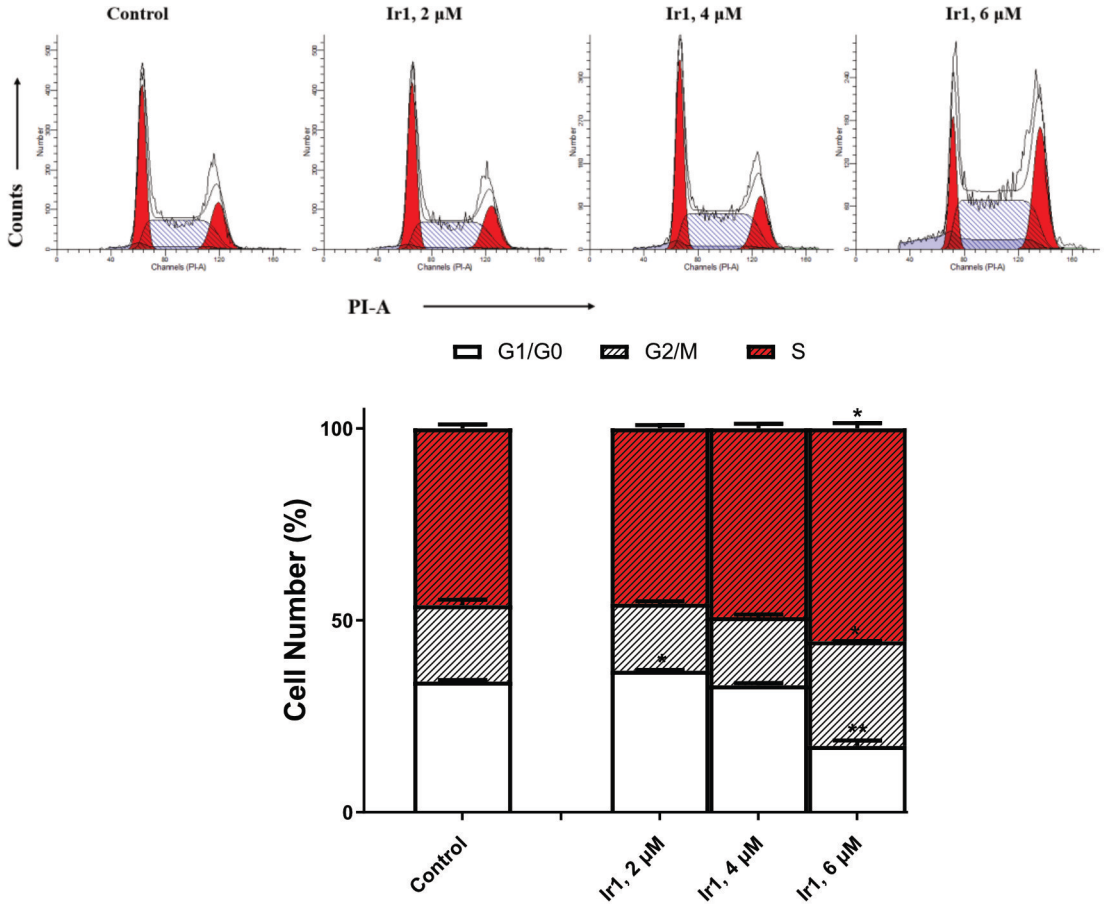

Figure 6. Effects of complexes **Ir1** on cycle distribution of HeLa cells. Cells were treated with **Ir1** at different concentrations for 24 h and analyzed by flow cytometry after PI staining (*$p < 0.05$, **$p < 0.01$, n = 9)

such as mitosis, apoptosis and autophagy.[37] Here we assessed HeLa cell viability after 24-hour **Ir1** treatment using the CellTiter-Glo® Luminescent Cell Viability Assay. As shown in Figure 7A, cell viability decreased to 52.95% at the highest concentration (6 μM **Ir1**) compared to the control (0 μM **Ir1**).

Mitochondrial physiological status was further evaluated using JC-1 dye, which shifts from red to green fluorescence in response to mitochondrial damage or depolarization.[38] **Ir1** treatment led to a concentration-dependent decrease in red fluorescence and a corresponding increase in green fluorescence, indicating mitochondrial depolarization and damage in HeLa cells (Figure 7B).

2.9. Tracking of Mitochondrial Viscosity via FLIM

The fluorescence lifetime of **Ir1** is linearly related to environmental viscosity. Using FLIM, we monitored dynamic changes in mitochondrial viscosity within HeLa cells following **Ir1** exposure. After 4 hours of treatment, a measurable increase in **Ir1** fluorescence lifetime was observed, showcasing its ability to track real-time changes in mitochondrial viscosity (Figure 8). The average fluorescence lifetime increased from 1748.88 ns to 2345.34 ns, corresponding to a rise in mitochondrial viscosity from 65.69 cP to 143.72 cP. These results align with previously reported data[39] and suggest a correlation between mitochondrial viscosity and physiological status.

3. Conclusions

In this study, we synthesized three iridium(III) complexes (**Ir1**-**Ir3**) containing 5-Fu, all of which demonstrated excellent photophysical properties. Among these, **Ir1** exhibited a specific response to environmental viscosity and effectively accumulated in mitochondria, enabling precise labeling of these organelles. Furthermore, **Ir1** retained the properties of 5-Fu by impairing cellular DNA function, blocking cell cycle progression and inducing apoptosis through caspase activation. Additionally, **Ir1** significantly disrupted mitochondrial energy and

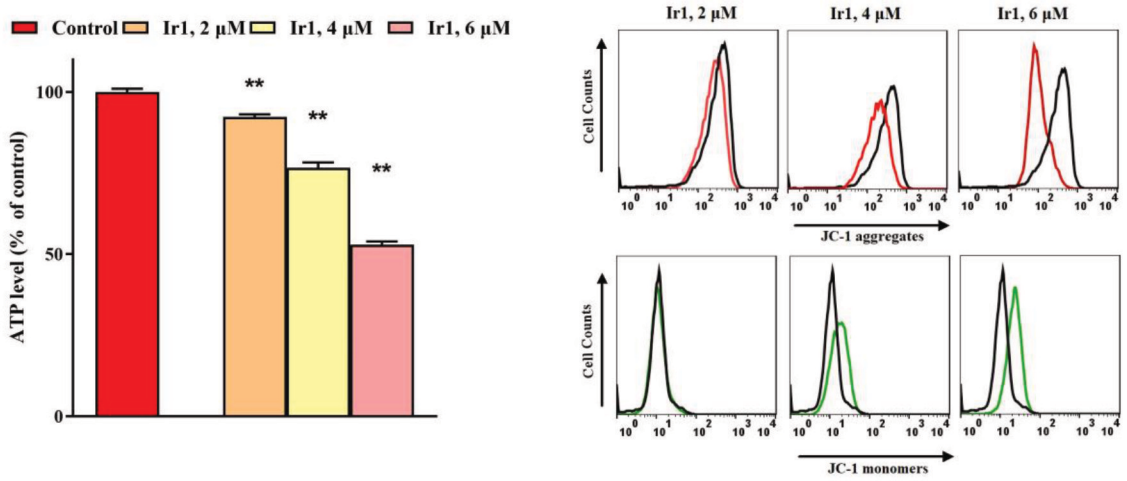

Figure 7. Effects of **Ir1** on mitochondrial integrity. (A) Intracellular ATP levels in Hela cells treated with **Ir1** at different concentrations for 24 h. (B) Cells were treated with **Ir1** at different concentrations for 12 h and analyzed by flow cytometry after JC-1 staining. (**$p < 0.01$, n = 9)

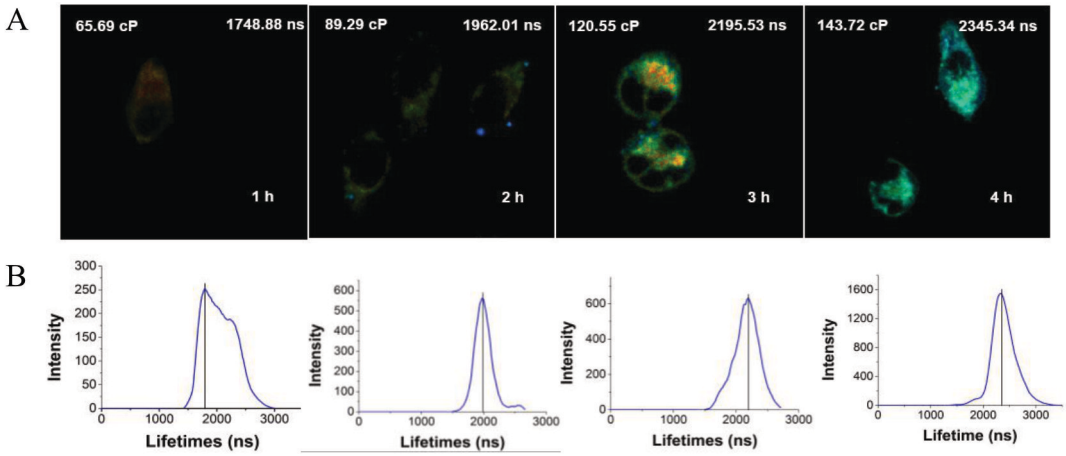

Figure 8. Mitochondrial viscosity in **Ir1**-treated HeLa cells detected by FLIM. HeLa cells were treated with **Ir1** (10 μM) and imaging at 1, 2, 3, and 4 h. ($\lambda_{ex} = 405$ nm, $\lambda_{em} = 600 \pm 20$ nm)

metabolic states, leading to increased production of mitochondrial ROS. Due to its highly sensitive fluorescence lifetime response to mitochondrial viscosity, **Ir1** is an effective tool for monitoring mitochondrial viscosity changes using FLIM. Our findings provide new insights into the development of small molecule-based anticancer drugs that not only induce therapeutic effects but also enable the real-time monitoring of microenvironmental changes at the subcellular level.

Acknowledgements

This work was funded by the Discipline Construction Project of Guangdong Medical University (4SG23004G), Key Scientific Research Projects of Colleges and Universities in Guangdong Province (2024ZDZX2070), Medical Industry Innovation Project of Guangdong Medical University (4SG22305P), and Medical Scientific Research Foundation of Guangdong Province (B2023240).

Conflict of Interests

The authors declare no competing financial interests.

Data Availability Statement

The data that support the findings of this study are available in the supplementary material of this article.

Keywords: Ir(III) complexes · Viscosity · Cytotoxicity · Antitumor · Mitochondria

[1] S. Dasari, P. B. Tchounwou, *Eur. J. Pharmacol.* **2014**, *740*, 364–378.
[2] B. Joshi, M. Shivashankar, *ACS Omega* **2023**, *8*, 43408–43432.
[3] Y. Liu, Y. Wang, X. Guan, Q. Wu, M. Zhang, P. Cui, C. Wang, X. Chen, X. Meng, T. Ma, *ACS Appl. Mater. Interfaces* **2023**, *15*, 26484–26495.
[4] Z. Zhao, P. Gao, L. Ma, T. Chen, *Chem. Sci.* **2020**, *11*, 3780–3789.
[5] J. Li, H. Chen, L. Zeng, T. W. Rees, K. Xiong, Y. Chen, L. Ji, H. Chao, *Inorg. Chem. Front.* **2019**, *6*, 1003–1010.
[6] M. H. Chen, Y. Zheng, X. J. Cai, H. Zhang, F. X. Wang, C. P. Tan, W. H. Chen, L. N. Ji, Z. W. Mao, *Chem. Sci.* **2019**, *10*, 3315–3323.
[7] J. Lyu, D. Liu, C. Wang, Z. Zhang, X. Zhang, *J. Mater. Chem.* **2022**, *B 10*, 6307–6314.
[8] M. Qian, D. Zhang, H. Qi, X. Yang, G. Yin, C. Zhang, J. Guo, H. Qi, *Chin. Chem. Lett.* **2023**, *34*, 107336.
[9] M. Hu, X. L. Zhou, T. X. Xiao, L. Hao, Y. Li, *Dalton Trans.* **2023**, *52*, 15859–15865.
[10] H. N. Kagalwala, J. Gerberich, C. J. Smith, R. P. Mason, A. R. Lippert, *Angew. Chem. Int. Ed.* **2022**, *61*, e202115704.
[11] M. Zeyrek Ongun, M. Sahin, S. Oguzlar, T. Akbal Aytan, S. Z. Topal, D. Atilla, *Inorg. Chim. Acta.* **2022**, *543*, 121197..
[12] G. G. Yang, Y. Q. Zhao, L. Zhang, S. Sun, B. Liu, X. Han, *Anal. Chem.* **2024**, *96*, 5931–5939.
[13] D. Chen, T. Shao, H. Zhao, F. Chen, Z. Fang, Y. Tian, X. Tian, *Dyes Pigm.* **2023**, *215*, 111271.
[14] P. Xiang, R. Huang, T. Shao, Y. Shu, D. Li, Q. Zhang, Y. Tian, X. Tian, *Chem.* **2022**, *361*, 131677.
[15] J. Zhou, J. Li, K. Y. Zhang, S. Liu, Q. Zhao, *Coord. Chem. Rev.* **2022**, *453*, 214334.
[16] Y. Ardeshirpour, V. Chernomordik, M. Hassan, R. Zielinski, J. Capala, A. Gandjbakhche, *Clin. Cancer Res.* **2014**, *20*, 3531–3539.
[17] B. B. Ganguly, N. N. Kadam, *Mitochondrion* **2022**, *65*, 88–101.
[18] X. Wu, R. Zhang, Y. Li, Y. Gai, T. Feng, J. Kou, F. Kong, L. Li, B. Tang, *Anal. Chem.* **2023**, *95*, 7611–7619.
[19] J. J. Liu, F. C. Meng, J. J. Lv, M. Y. Yang, Y. M. Wu, J. Gao, J. J. Luo, X. M. Li, G. Wei, Z. L. Yuan, H. Y. Li, *Spectrochim. Acta Part A* **2023**, *295*, 122602.
[20] C. Zong, Q. Lu, J. Niu, F. F. Meng, X. Q. Yu, *Spectrochim. Acta Part A* **2023**, *299*, 122883.
[21] S. J. Park, B. K. Shin, H. W. Lee, J. M. Song, J. T. Je, H. M. Kim, *Dyes Pigm.* **2020**, *174*, 108080.
[22] H. Leng, J. Yang, L. Long, Y. Yan, W. J. Shi, L. Zhang, J. W. Yan, *Bioorg. Chem.* **2023**, *136*, 106540.
[23] S. J. Li, Y. F. Li, H. W. Liu, D. Y. Zhou, W. L. Jiang, J. Ouyang, C. Y. Li, *Anal. Chem.* **2018**, *90*, 9418–9425.
[24] N. L. Pan, Y. Q. Zhang, M. Y. Huang, Z. J. Liang, Y. Gong, X. D. Chen, Y. L. Li, C. L. Wu, Z. N. Huang, J. Sun, *J. Biol. Inorg. Chem.* **2024**, *29*, 265–278.
[25] Z. G. Yang, Y. X. He, J. H. Lee, N. Park, M. Suh, W. S. Chae, J. F. Cao, X. J. Peng, H. Jung, C. Kang, J. S. Kim, *J. Am. Chem. Soc.* **2013**, *135*, 9181–9185.
[26] L. Wang, Y. Xiao, W. M. Tian, L. Z. Deng, *J. Am. Chem. Soc.* **2013**, *135*, 2903–2906.
[27] R. C. Taylor, S. P. Cullen, S. J. Martin, *Nat. Rev. Mol. Cell Biol.* **2008**, *9*, 231–241.
[28] T. N. A. Pham, B. Le, S. H. Yang, *Biotechnol. Bioeng.* **2021**, *26*, 63–70.
[29] J. Thorburn, L. M. Bender, M. J. Morgan, A. Thorburn, *Mol. Biol. Cell* **2003**, *14*, 67–77.
[30] S. M. Man, T. D. Kanneganti, *Nat. Rev. Immunol.* **2016**, *16*, 7–21.
[31] Y. Zheng, L. He, D. Y. Zhang, C. P. Tan, L. N. Ji, Z. W. Mao, *Dalton Trans.* **2017**, *46*.
[32] J. Jun, C. Cao, *Chem. Sci.* **2017**, *8*, 631–640.
[33] Y. Yang, L. Guo, X. Ge, T. Zhu, W. Chen, H. Zhou, L. Zhao, Z. Liu, *Inorg. Chem.* **2020**, *59*, 748–758.
[34] X. Ge, S. Chen, X. Liu, Q. Wang, L. Gao, C. Zhao, L. Zhang, M. Shao, X.-A. Yuan, L. Tian, Z. Liu, *Inorg. Chem.* **2019**, *58*, 14175–14184.
[35] C. M. Wang, C. Ploia, F. Anselmi, A. Sarukhan, A. Viola, *EMBO J.* **2014**, *33*, 1354–1364.
[36] T. W. Peters, A. W. Miller, C. Tourette, H. Agren, A. Hubbard, R. E. Hughes, *G3 (Bethesda)* **2016**, *6*, 161–170.
[37] K. Ratajczak, A. Lukasiak, H. Grel, B. Dworakowska, S. Jakiela, M. Stobiecka, *Anal. Bioanal. Chem.* **2019**, *411*, 6899–6911.
[38] Y. Li, C. P. Tan, W. Zhang, L. He, L. N. Ji, Z. W. Mao, *Biomaterials* **2015**, *39*, 95–104.
[39] L. Hao, Z. W. Li, D. Y. Zhang, L. He, W. Liu, J. Yang, C. P. Tan, L. N. Ji, Z. W. Mao, *Chem. Sci.* **2019**, *10*, 1285–1293.

Manuscript received: September 15, 2024
Revised manuscript received: November 6, 2024
Accepted manuscript online: November 8, 2024
Version of record online: November 23, 2024